8-2010

Automated procedures for quantification of rhizosphere physical properties in micro CT images

Natarajan S. Pillai
University of Nevada, Las Vegas

AUTOMATED PROCEDURES FOR QUANTIFICATION OF RHIZOSPHERE PHYSICAL PROPERTIES IN MICRO CT IMAGES

by

Natarajan Sivathanu Pillai

Bachelor of Technology in Electronics and Communication Engineering
Anna University, Chennai, India
May 2006

A thesis submitted in partial fulfillment
of the requirements for the

Master of Science Degree in Electrical Engineering
Department of Electrical and Computer Engineering
Howard R. Hughes College of Engineering

Graduate College
University of Nevada, Las Vegas
August 2010

ABSTRACT

Automated Procedures for Quantification of Rhizosphere Physical Properties in Micro CT Images

by

Natarajan Sivathanu Pillai

Dr. Emma E. Regentova, Examination Committee Chair
Associate Professor of Electrical and Computer Engineering,
University of Nevada, Las Vegas

The rhizosphere, i.e. the zone of soil immediately surrounding plant roots plays a prominent role in supplying plants with water and nutrients. However, surprisingly little is known about rhizosphere physical properties and how they affect root growth, water and nutrient uptake. The lack of non-invasive and non-destructive imaging techniques necessary to observe living roots growing in undisturbed soil have been a main reason for this shortcoming. Recent advances in synchrotron X-ray micro tomography (CMT) provide the potential to directly observe soil physical properties around living roots in-situ.In this work we develop procedures for assisting scientist to study the soil properties by visualizing and automatically processing micro CT images. Specifically image de-noising in the wavelet domain is performed for convenient profiling and segmentation is applied for automated calculation of soil properties. As new measures we proposed the normalized radial and circular aggregation and water transportability and also have shown ways of generalizing the studies for 3D.

ACKNOWLEDGMENTS

It’s a great opportunity to express honor to all my dear ones. I owe my deepest gratitude to my Advisor Dr. Emma Regentova, who apart from helping me to shape this thesis, have also been an indispensable person who helped me stand by my vision. I would always thank Dr.Peter Allen Stubberud for his sincere efforts in teaching and making me a valued Electrical Engineer. I would like to thank Dr.Ajoy Datta for being a part of advisory committee. Thanks would not be enough to express my sincere gratitude to Dr. Henry Selvaraj who in his role has always been there for my best interests, failures, efforts, requests and guiding me with all his altruistic efforts.

I would like to thank my scientific advisor Dr. Markus Berli, for his constant force in all my endeavors to groom me as a graduate student. It is from him, I learnt empathy, compassion, patience, love, the power of listening, discipline, remarkable team work, also influenced by his integrity and accountability. Now, I would like to thank all my faculty members and students of DRI, UNLV, NSF and its committee members, NSCEE, LBNL for their direct and indirect support in this thesis. Also i owe my sincere thanks to Dr. Evangelos A.Yfantis for his motivation, Dr.Muthukumar Venkatesan, Dr.Rama Venkat for being a great source of inspiration. I would always thank Ajay Kumar Mandava for helping me to form this thesis.

I would like to thank my brother Madhavan Sivathanu Pillai for his innate affection. I thank all my family members for having infused me with the value of higher education and all my friends for their priceless contribution. I would like to thank my dear cousin Dr.Subramanian Vallinayagam Pillai, for he served as an inspiration to set my foot in the quest of knowledge. Finally I thank god for blessing me with an ever blissful and peaceful life.

TABLE OF CONTENTS

LIST OF FIGURES

CHAPTER 1

INTRODUCTION

1.1 Scientific Motivation

The rhizosphere, i.e. the zone of soil immediately surrounding plant roots [1], plays a prominent role in supplying plants with water and nutrients [2, 3]. Despite their importance, surprisingly little is known about rhizosphere physical properties and how they affect root growth, water and nutrient uptake [4-6]. The lack of non-invasive and non-destructive imaging techniques necessary to observe living roots growing in undisturbed soil have been a main reason for this shortcoming. Recent advances in synchrotron-based X-ray micro tomography (XMT) provide the potential to directly observe soil physical properties around living roots in-situ [7]. Fig. 1.1 shows the example of a sunflower root growing in a bed of glass beads, representing a simple type of soil [7]. In Figure 1.1, pore structure, pore fluid phases as well as a plant root are clearly visible. In order to further explore the physics and mechanics of the rhizosphere from XMT images, image information (e.g. gray value of each pixel of a XMT image) has to be converted into physical information such as soil solid, liquid, gas, root tissue that in turn can be converted into soil physical parameters (e.g. porosity, pore size distribution, hydraulic conductivity). So far, there are no tools available to do this objectively and in a semi-automatic manner so larger amounts of images can be processed.

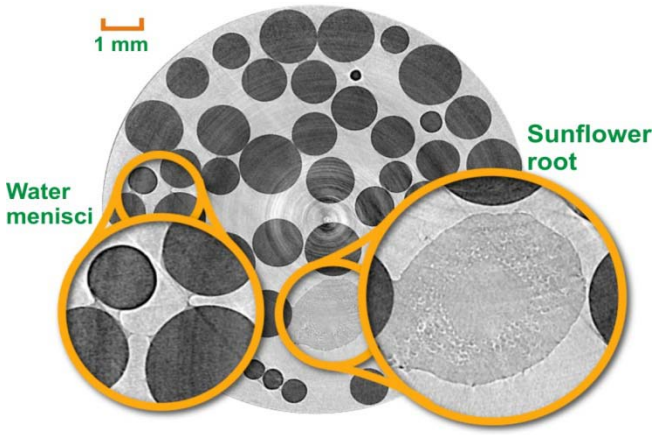

Figure 1.1: Sunflower root (H. annuus) growing in glass beads imaged by using synchrotron X-ray Micro-Tomography (XMT). Zoomed areas show water menisci and root structure [7].

1.2. Non-destructive imaging by Computed Tomography (CT)

Computed Tomography (CT) has been an effective means for non–destructive imaging of solid materials. Comprehensive reviews on CT studies in earth science have been carried out by Ketcham et al. [8]. They found that CT is an excellent tool to perform *in-situ* visualization of geomaterials in a non-invasive and non-destructive manner. The most common forms of CT in material sciences are X-ray CT and Neutron Tomography (NT) [9]. X-ray CT is sensitive to a material atomic number, and hence, the CCD detects density differences within a solid body [8]. For X-ray CT, polychromatic X-ray sources are employed to scan larger objects (centimeter to meter scale) in industrial scanners while monochromatic synchrotron radiation is used as an X-ray source for micro CT applications at the micrometer to mm scale (XMT). NT is sensitive to hydrogen atoms and is predominantly used to detect hydrogen-rich substances in solid bodies (water,

organic matter) [10][9]. Every method is pervasive in a different field of application depending on application requirements. Industrial X-ray CT has the potential to scan large objects but at the costs of smaller spatial resolution as well as issues like beam hardening effects. Synchrotron-based high resolution XMT, on the other hand, is limited to really small objects. NT has the potential to directly observe distribution of water or organic substances but is limited by spatial resolution (~0.1mm) and needs a nuclear reactor as a neutron source.

Therefore CT imaging has been widely used in the geoscience community to quantify physical properties of soil and rock, their structure and chemical composition [11]. Among these properties are porosity [12], saturation [12], solid surface area [12], the interfacial area between fluid phases [12], fluid distribution between porous materials [13] and their interfacial dynamics[11], dense non-aqueous phase liquid transport [12], fluid process flow [13], grain/pore size distribution [14], storage of water, transportation of hazardous substances [14], connectivity between pores [12], grains/aggregates and flow rate (fourth dimension) [13], residual saturation [13], capillary pressures [13], interface curvature area [12], as well as 3-phase contacts and permeability [12].

Recent advances in CT-based non-destructive imaging have already have been used to provide snapshots of root architecture, pore geometry, and bulk soil structure using X-ray radiography [15-17], neutron radiography [18, 19], or magnetic resonance imaging [20]. X-ray Micro-Tomography (XMT) has been employed successfully for root growth investigations [21, 22] and synchrotron-based XMT for mapping the distribution of elements in plants [23].

The overarching goal of our study is to use synchrotron-based XMT to gain improved insight into rhizosphere structure as well as root-induced physical transformations in the rhizosphere. Synchrotron-based XMT has the potential for obtaining images at spatial resolutions down to 1 μm for both materials with clearly different X-ray attenuation (e.g., solid particles and air-filled pores) as well as for materials of similar X-ray attenuation (e.g., water and root cell tissue, air-water interfaces) simply by adjusting the X-ray beam energy level.

For CT imaging, we had access to the Advance Light Source of the Lawrence Berkeley National Laboratory (LBNL). This facility uses a Synchrotron X-ray source (1.9 GeV), superbend magnet (4.37 Tesla), and multilayer monochromator to deliver a monochromatic beam with an adjustable energy range from 5 to 60 keV to the specimen (beam size 40×4.6 mm). Transmitted X-ray light is converted to visible light using a $CdWO_4$ single crystal scintillator, magnified by a Canon 2X lens, and imaged on a Cooke PCO 4000 CCD camera.

Scans are carried out by placing a specimen in between the source and detector (Fig.1.2a). For our experiments, specimens were prepared by planting seeds in soil filled in small glass test tubes of 10mm inner diameter (Fig. 1.2b).Seeds and soil were sufficiently watered for the seeds to germinate and grow a tap root large enough so that soil-root interactions could be observed. The process is varied for different soils and different seeds including dry and wet conditions [for details, see 7].

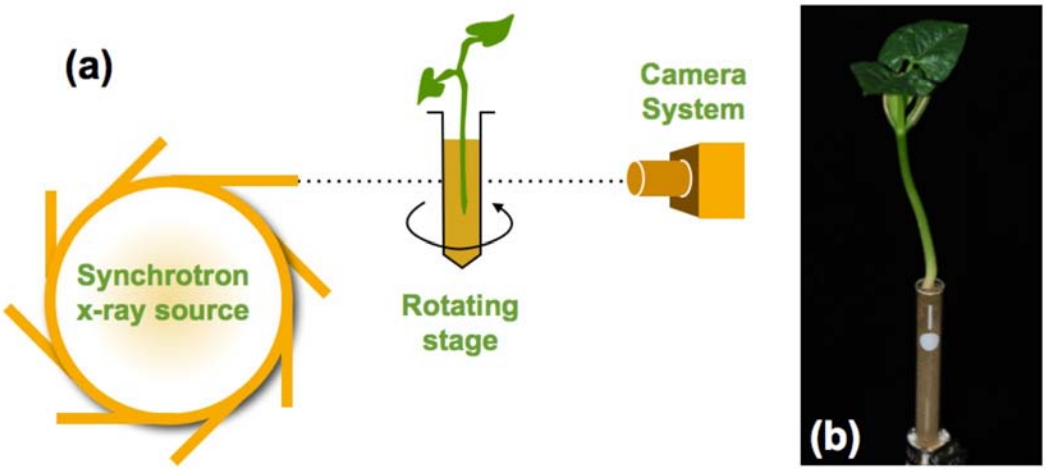

Figure 1.2: (a) Schematic depiction of the XMT setup at the Advanced Light Source, Berkeley California, (b) soil-filled glass test tube for growing plants [7]

In our beamline setup, the source and detectors are fixed but the specimen is rotatable. For the cross section images as shown in Figure 1.1, 720 exposures were taken per scan at 0.125° incremental angles yielding a final voxel size of 4.4 μm side length. The number of images recorded affects the quality of image. As per the Beer's law, the density transitions in the images correspond to the boundary lines of different objects. For proper XMT image acquisition, a number of issues have to be taken into consideration [8].

Before each scan, calibrations have to be run to map the minimum and maximum range for reconstruction of the sinogram (values of every angular orientation) that corresponds to attenuated beam values. The number of views and the rotational interval from top to bottom determines the spatial resolution, so certain parameters have to be adjusted before every beam time run as the specimen composition could differ. Special calibrations are done for desired imaging output. Desired image output means the objects in the specimen that are particularly under study are fairly distinguishable to both human

perception and computerized automata. Though postprocessing is involved after image reconstruction, a procedure such as wedge calibration seems amenable to attain perfect 3D images or slices.Image reconstruction is typically performed using a method called filtered back-propagation[24]. Laks and Logan [8] are the filters designed for the images after reconstruction at the expense of spatial resolution [8]. The reconstructed image suffers from artifacts such as partial volume effects and beam hardening, ring artifacts and other artifacts like the high density material exhibiting as 'starbust'. The Starbust is defined as an artifact that affects the CT value of neighboring pixel.

Usually a reconstructed image carries a spatial resolution that roughly varies from 3000 to 4000 pixels. If each pixel is represented by 16 bits, the total size of the image would vary from 30MB to 40MB. Therefore, a stack of slices are available for 2D image processing, quantification and 3D visualization. The acquired images can be processed in 2D and 3D. Due to the limitations of processing power and memory storage, the images were usually processed slice by slice in a 2D fashion. Also the advent of high performance computing has given room for processing data in 3D and in the temporal fashion (4D).

The objective information available at this micro scale is provided though the huge amount of data. These data carry vigorous information about the soil structure, root structure and its rhizosphere. Though these materials and structures are seen visually, there is a need to study the behavior, the interaction of aggregates, grains with fluids, the phases and its temporal transformation due to evaporation, saturation and the root growth. Since the amount of information is huge, any kind of analysis needs several man hours to view the data and to extract useful information and observe characteristics. Therefore

automated procedures are demanded to assist scientist with both viewing images in a convenient format and extracting information for quantifying properties important for their studies.

1.3 Image Processing and Analysis: Problem Formulation, Objectives and Tasks

1.3.1 Problem Formulation

The problem of quantifying soil physical properties around a root has been addressed by Berli et al. (2010) but only based on an expert judgment, manually and by using global thresholding as a segmentation technique. The approach by Berli et al. (2010) works for an individual image but is tedious and strongly depends on the expert's knowledge and skills to identify and delineate image features. In addition, global thresholding has been proved to have limited applicability for soils since in general no clear distinction between solids and pores in the histogram of the grey scale image is possible [11].

A review by Porter and Wildenschild [12] showed that various tools and open source software for 2D and 3D and image processing and analysis do already exist. Most of these tools, however, were originally designed for medical images and have limited applicability to analyze rhizosphere physical properties objectively and semi-automatically. So there is no "off-the-shelve" solution available. To obtain physical information (soil, solid, liquid, gas, root tissue) from the "raw" XMT grayscale images acquired at the Advance Light Source of the Lawrence Berkeley National Laboratory (LBNL), a number of pre-processing and segmentation issues have to be addressed.

X-ray imagery has an inherent noise due to wave scatter. Additionally, soil materials typically have a wide range of component density. Especially strong attenuation due to high-density particles (e.g. metal ore) hinders segmentation, and subsequently image

analysis. Fig.1.1 shows one slice of the stack data with very bright components indicating high absorption by metallic or concrete components. Aggregates may vary in their density and pores can be saturated or non-saturated. For obtaining objective measures useful for soil physics, filtered images are *segmented*, that is areas of the image representing different densities, such as soil pores, particles, aggregates and roots are to be delineated. Several segmentation and thresholding techniques have already been applied to soil microCT as reviewed by Sezgin et al. [25] and Iassonov et al. [5]. The choice of segmentation after the appropriate enhancement filters has urged the signal processing experts to design algorithms that adapt and segment the image data based upon the texture or using generic clustering algorithms [11]. Reviews show that several algorithms which have been designed for segmentation of geoscience related image data [8] show significant improvements [11]. The increase in the spatial resolution demands higher computational requirements without producing credible results. However, this uncorrelated output with respect to the increase in spatial resolution has to be validated. Also the problem of segmenting the air-water (wet and dry surfaces) has proved to be challenging. The processing of image pixels slice by slice in 2D has significant loss of features/information, so the recent developments in porous media studies were performed on voxels as 3D [11].

1.3.2 Objectives and Tasks

The objective of this study is to develop tools to objectively de-noise, segment and analyze XMT images in order to quantify rhizosphere physical properties (porosity, pore size distribution, hydraulic conductivity).

To reach this goal, the following tasks were carried out in this work.

1. Data preprocessing and visualization for conventional visual analysis.
2. Image segmentation as a preprocessing step for automated data analysis
3. Data Quantification based on segmented images

To get an overview of the task, refer the flow diagram from Fig 1.3

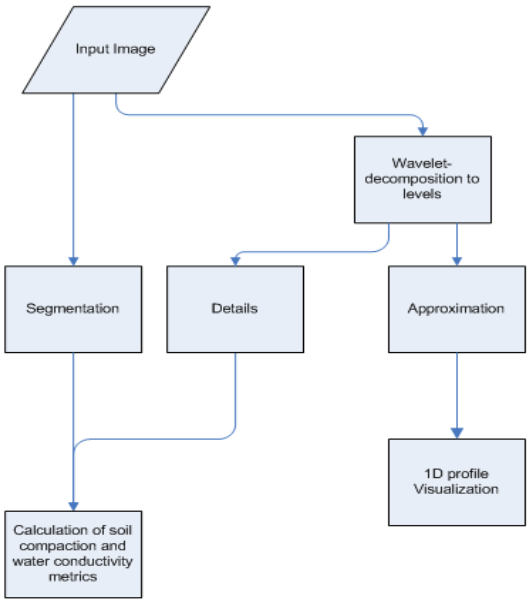

Fig 1.3 Flow diagram

In this work we approach image analyses using

(a) Wavelet multi-resolution decomposition

(b) Combination of automated and interactive procedures for obtaining segmented images at a desired level of image abstraction.

We propose new metrics to measure soil porosity and pore size distribution that are available to be computed spatially at any region and globally and We also evaluate hydrological conductivity based on the analysis of segmented images. We also visualize

data facilitating more efficient and convenient analyses by a human expert. The work also poses certain research problems and shows research directions and open problems.

The work is outlined as follows. Chapter 2 presents early results of de-noising and visualization of intensity profiles. In Chapter 3, we analyze segmentation techniques for selecting best candidates for the goals of our research. Chapter 4 presents new quantitative measures obtained on segmented and post-classified data. Chapter 5 concludes the work and discusses possible future directions in this research area.

CHAPTER 2

ENHANCEMENT AND VISUALIZATION

2.1 Image Preprocessing for Intensity Profiling

One of the basic methods for studying the aggregate/pore distribution is the analysis of intensity profiles. Usually this is performed by indicating end-point coordinates of a line along which the intensities are concerned and plotting the intensity distribution. There are two problems associated with such profiling. First is the texture content of all components of the images such as pores, aggregates and the root. Secondly, 16-bit image and non-linear characteristics of CCT camera naturally lead to a certain level of noise. That complicates both visual and automated analyses. An example of intensity profile along a specified line on the original (Fig.2.1) is shown in Fig.2.2.

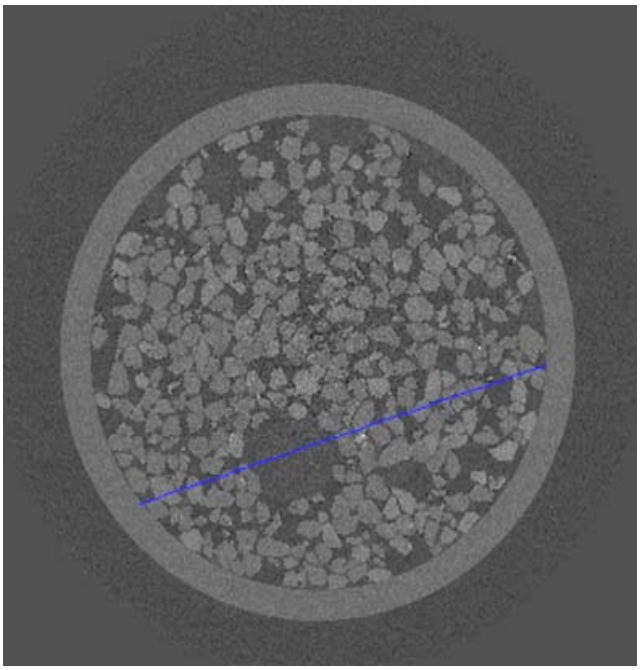

Fig.2.1. A microCT image of a container with a root and soil (aggregates are of lighter intensities). A line across the container image is indicated by a scientist for obtaining the intensity profile.

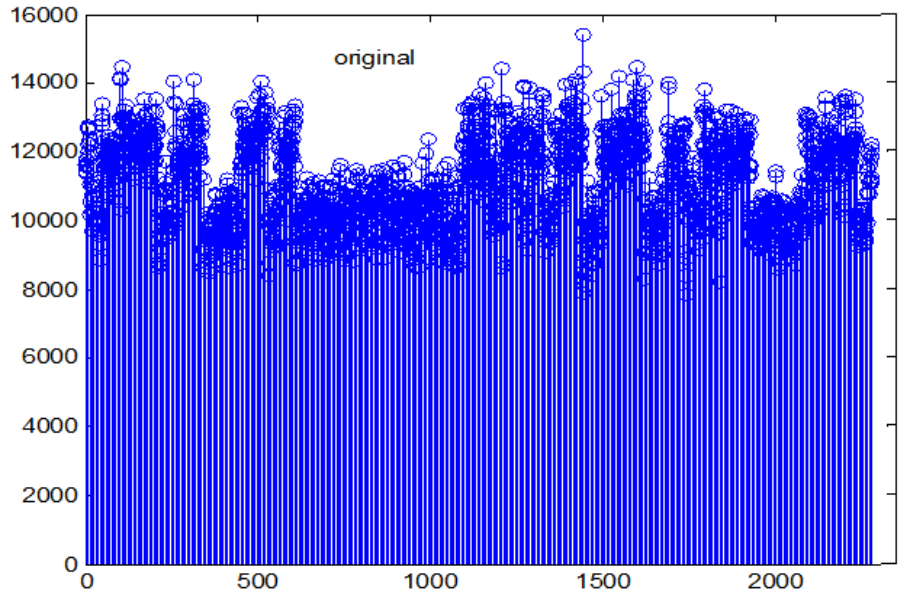

Fig.2.2. Intensity profile along the line depicted in Fig.2.1

From the profile in Fig.2.1, it is hard to judge how many aggregates the line passes through. So the objective is to obtain a smoother profile, i.e., one which neglects the texture variations of aggregates and pores.

In this Chapter, we show how to exploit wavelet multiresolution decomposition for attaining a more convenient way of representing the intensity profile and show approaches of utilizing the result for studying aggregate/pore distribution. The two types

of transforms considered, are decimated and stationary (undecimated) wavelet transforms.

2.2. Wavelet shrinkage

2.2.1 Mathematical Preliminaries

In this section, we briefly discuss the properties of the wavelet transform. A more detailed explanation can be found in [26] .

Wavelet decomposition represents a signal by means of a finite length oscillating wavelet function, which is scaled and translated (shifted) to match the input signal. The wavelet function, called a mother wavelet has to satisfy the following conditions.

$$\int \psi(t)dt = 0 \quad \text{and} \quad \int_{-\infty}^{\infty} \psi^2(t)dt = 1.$$

Bases functions are produced by scaling (or dilating) the mother wavelets by a factor of *a* and translating it by a factor of *b*.

$$\psi_{a,b}(t) = \frac{1}{\sqrt{a}}\psi\left(\frac{t-b}{a}\right)$$

Hence, the transform realizes both time and frequency representation by capturing frequency content at different scales and times at which these frequencies happened. The following properties of the wavelet transforms make them attractive for image analysis.

Locality: Each wavelet coefficient represents the image content localized in a spatial location and a frequency.

Multiresolution: Wavelet transform analyzes the image at a nested set of scales.

Energy Compaction: The wavelet transforms of real-world images tend to be sparse. A wavelet coefficient is large only if singularities are present within the support of the

wavelet.

Decorrelation: The wavelet coefficients of real-world images tend to be approximately decorrelated.

Many researchers have contributed to the formulation of the transform set. The Daubechies' formulation is based upon the use of recurrence relations to generate progressively coarser discrete samplings of an implicit mother wavelet function, each resolution being twice that of the previous scale. Due to their properties, Daubechies' wavelets produce remarkable results for image analysis and synthesis problems. The wavelets have a compact support; thus, they can be easily implemented by finite length filters. This finite length property is important for spatial domain localization. Furthermore, functions with continuous derivatives allow continuous signals to be analyzed more efficiently. Additionally, edge artifacts can be avoided.

In general, a continuous wavelet transform operating over every possible scale and translation is more efficient for image analysis. The discrete wavelet transform (DWT) uses only a specific subset of all scale and translation values .

The DWT of a signal x[n] can be calculated through implementation of a filter bank by a QMF-quadrature mirror filter.The Signal is passed simultaneously through a lowpass filter with an impulse response g[n] and a highpass filter with an impulse response h[n].

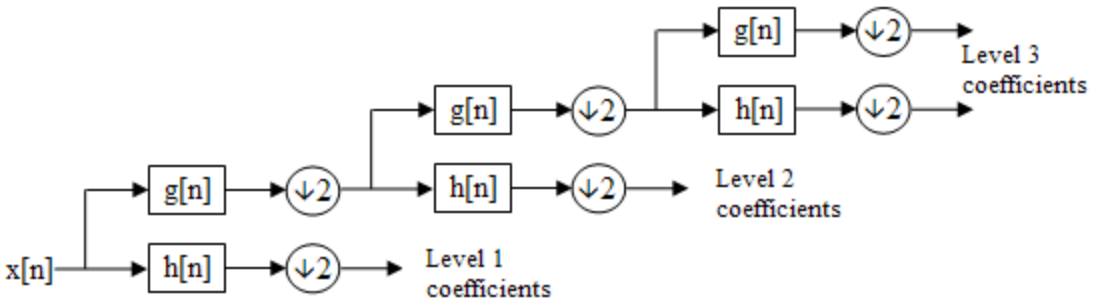

Fig.2.3 DWT (decimated)

Since each half of the signal's frequency domain has been represented in one of the two channels, a half of the samples can be discarded. The above process can be repeated for a finite number of levels, k. The resulting outputs of the high-pass filter are details and that of low-pass filter is the approximation of the signal. This constitutes the process of a decimated dyadic wavelet transform.

The wavelet function is used as a high-pass filter, and the scaling function as a low-pass filter. The following Fig. 2.4 shows the Daubechies' 4 (db4) wavelet and scaling functions that we use in this work

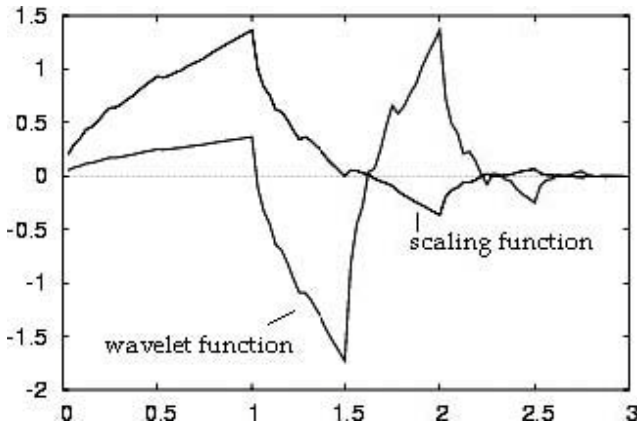

Fig.2.4 db4 wavelet and scaling function.

The choice of the function is substantiated by the nature of the signal which exhibits smooth variations across the image.

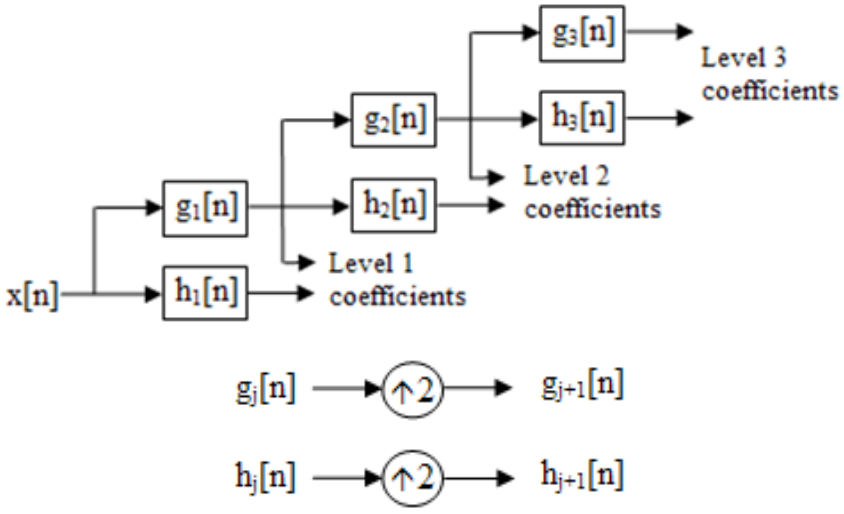

Fig.2.5 SWT

A drawback of the dyadic transform is the resolution change. An undecimated transform does not involve down sampling step, and thus preserves the original resolution of the image. For the application, this can be considered a useful property which allows for in-place visualization and calculations.The undecimated, a.k.a. stationary wavelet transform- SWT is performed as shown in Fig. 2.5

2.2.2 Hard- and soft-thresholding algorithms

The thresholding technique serves as a powerful mathematical tool and lends itself to applications such as denoising, visualizing data at different scales, and thus removing certain undesired frequencies. The wavelet coefficients calculated by a wavelet transform represent changes in the time series at a particular resolution. By looking at the time series in various resolutions it should be possible to filter out noise. A method to calculate the threshold is explained below.

1. Calculate a wavelet transform and order the detail coefficients by increasing frequency.
2. Calculate the *median absolute deviation* (MAD) of the detail coefficients spectrum. The

median is calculated from the absolute values of the coefficients.

3. Calculate the noise threshold from the following equation

$T_l = \frac{1}{0.6745} * MAD * \sqrt[2]{2 * \log_x N}$,

where

T_l- Threshold value calculated at every level

MAD - Median Absolute Deviation.

x - Log base.

N – Length of the coefficients or size of the time series

MAD is calculated as follows. In order to find a threshold for 1D, we use the following formula.

MAD = Median (abs ($Coeff_{ijl}$)) where

$$Coeff_{ijl} = \begin{cases} i = 1, j = 1{:}N, l - level, & 1D \\ i = 1{:}M, j = 1{:}N, l - level, & 2D \end{cases}$$

M is the number of rows, N is the number of columns of the coefficients considered at level 'l' and 0.6745 in the denominator rescales the numerator, and it is an estimator for the standard deviation for Gaussian white noise [2].

4. Threshold the detail coefficients.

There are two popular versions of thresholding algorithms

Hard thresholding sets any coefficient less than or equal to the threshold to zero. Other coefficients are preserved.

$$if(T > abs(Coeff_{ijl}))$$

$$CoeffH_{ijl} = 0;$$

Soft thresholding subtracts the threshold from any detail coefficient that is greater than the threshold. This moves the time series toward zero.

$$if(T > abs(\ Coeff_{ijl}\ ))$$

$$CoeffS_{ijl} = 0;$$

else

$$CoeffS_{ijl} = T - \ Coeff_{ijl}\ ;$$

If de-noising the image is of prime interest, after thresholding, one can implement the inverse transform and reconstruct the image which is noise-free.

The goal of this study is to preserve the magnitude of significant coefficients as an indicator of the strength of the intensity change, so the application can afford only the hard thresholding. The approximation and detail coefficients now contain important information of the signal and its variations and can be further analyzed by an expert.

2.2.4 Profiling at different resolution levels

There are two approaches to thresholding, One uses a 1D transform along a line of interest and the second exploits the 2D transform performed by applying filters sequentially to image rows and then to columns. The expected benefit of the 2D approach is the use of available statistics gleaned from the whole image. Additionally, a 2D transform yields details indicating the intensity changes in one of three directions - vertical, horizontal and diagonal. The flow chart of both approaches is shown in Fig. 2.6.

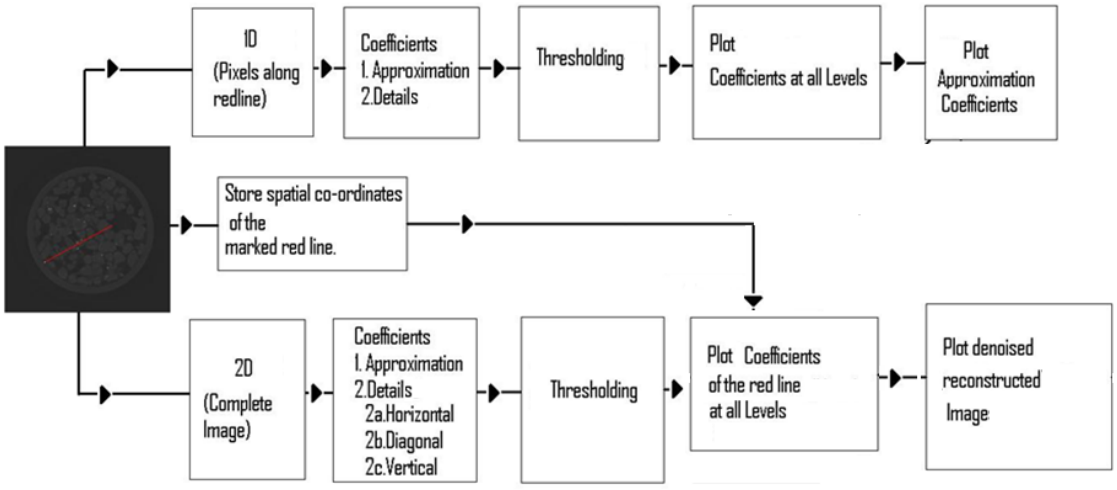

Fig.2.6 Flow chart of 1 and 2D approach of intensity profiling.

The 1D transform is performed with a db4 filter using dyadic transform and Stationary Wavelet Transform (SWT) is performed on the whole image. Different levels of approximation can be required for studying the soil properties through gray-scale image profiling. The maximum number of levels can be determined based on the length of the line. The algorithm proceeds as follows:

1. Find the length of the line in pixels, L.
2. Obtain k= $\log_2$ L. Round the result to a nearest integer. Example , L=130, k=$\log_2$130 =8
3. Decrement the obtained number by 1; for example m=k-1=8-1=7.
4. If $2^m \geq 32$, Go to Step 5; otherwise, plot the original intensities. Stop.
5. Take 2^m pixels on the line and apply one level of transform.
6. Plot approximation and detail coefficients of level m. Decrement m. Goto Step 4.

Results of the application of the 1D DWT transform to the original image with a line profile as shown in Fig.2.7 are displayed in Figures 2.8 through 2.11. We plot only

phases of thresholded transform coefficients indicating the intensity change direction, that is high-low (-1) or low-high (+1), rather than the actual values which indicate magnitudes of the intensity change. This represents information useful for calculating a number of components along the line, inter-components distances and the length of the aggregates cross sections.

It can be seen that although the approximation provides a smooth version of original signal,the threshold is not accurate enough for preserving all important edges. We believe that this happens due to the lack of statistics of the image, and therefore we apply 2D SWT to the whole image and plot only coefficients in spatial coordinates of the line for comparison. The plot of thresholded coefficients is based on the following logic that if either one of the vertical or diagonal or a horizontal coefficients are above the threshold then the value of the coefficients are retained else the value is zeroed out and then the phase is plotted. The results are shown in Figures 2.12 through 2.15.

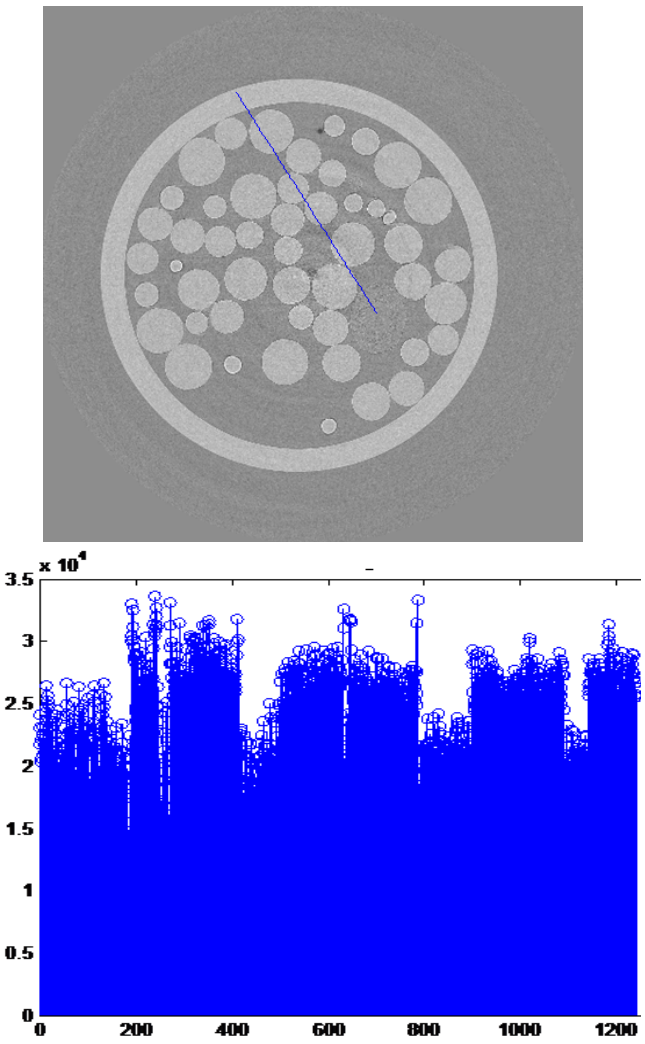

Fig.2.7. (top): microCT of a container with glass beads in the water; (bottom) the profile along the selected line

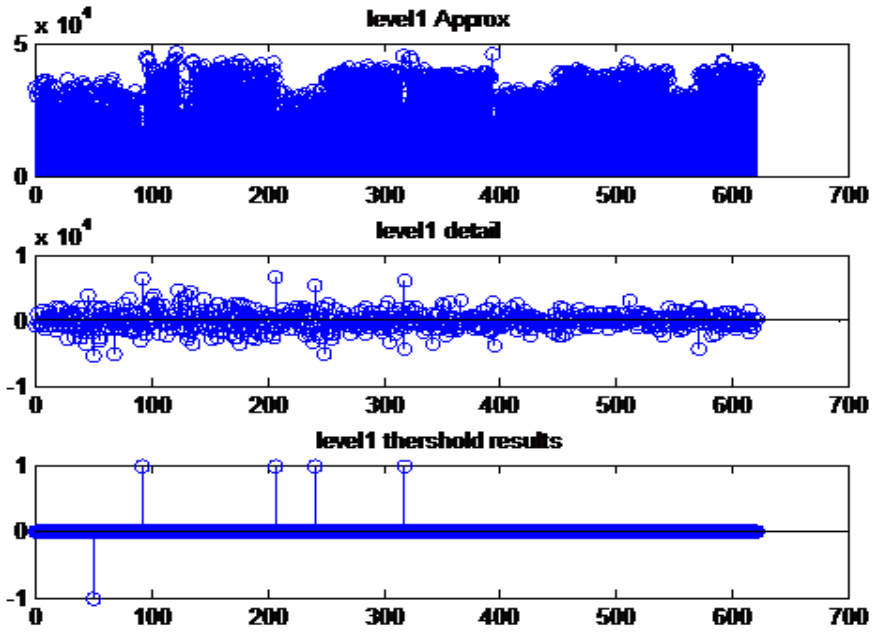

Fig.2.8 Level 1 of the transform

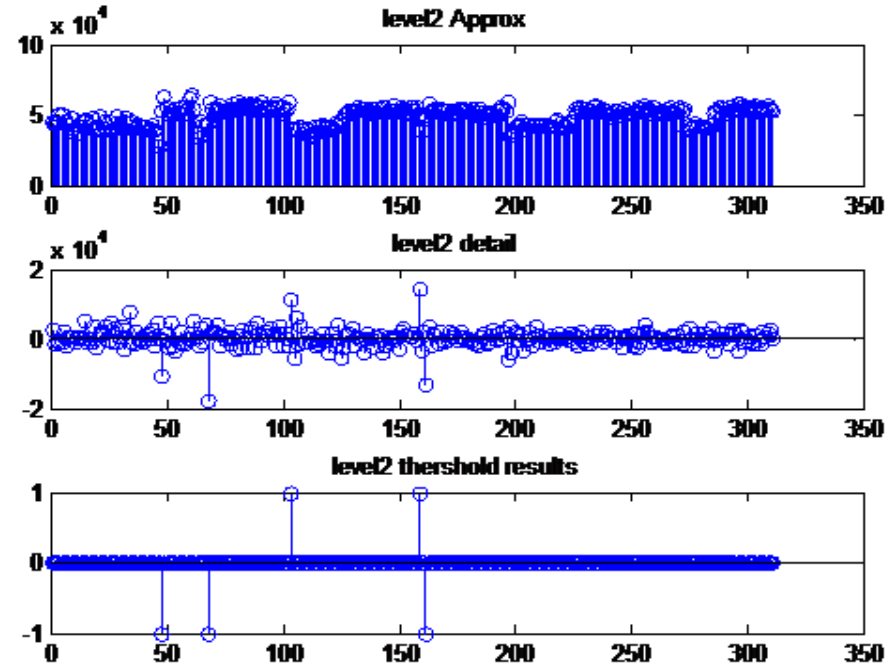

Fig.2.9 Level 2 of the transform

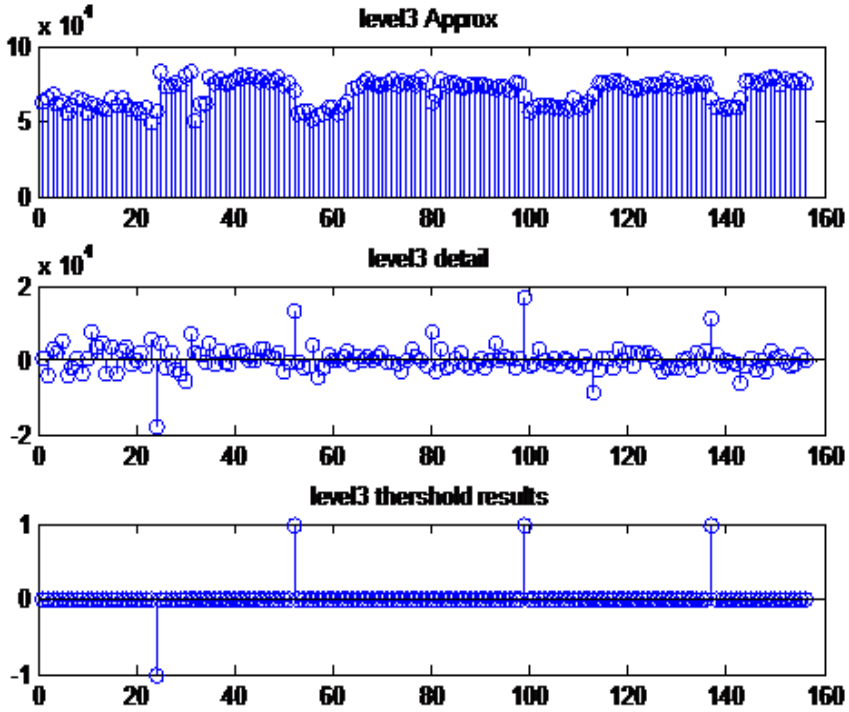

Fig.2.10 Level 3 of the transform

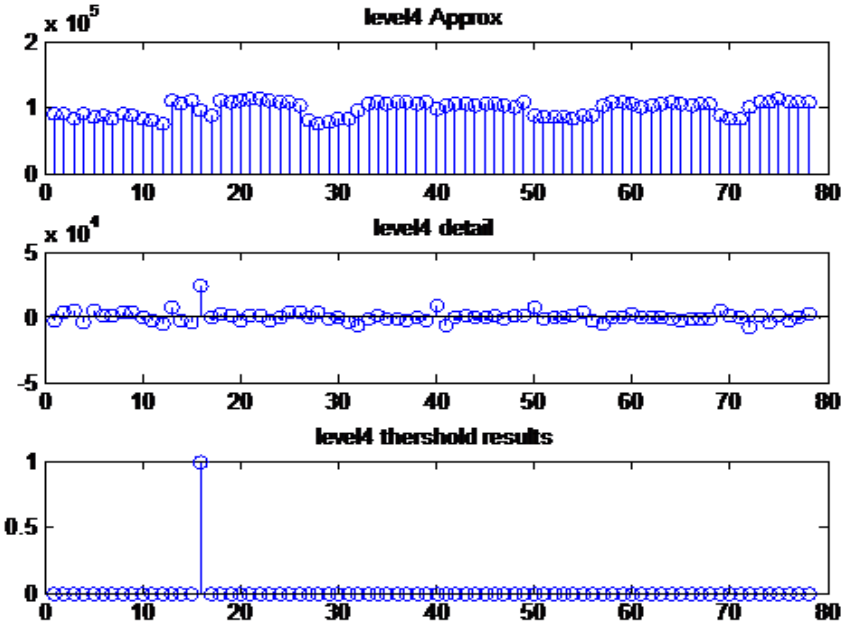

Fig.2.11 Level 4 of the transform

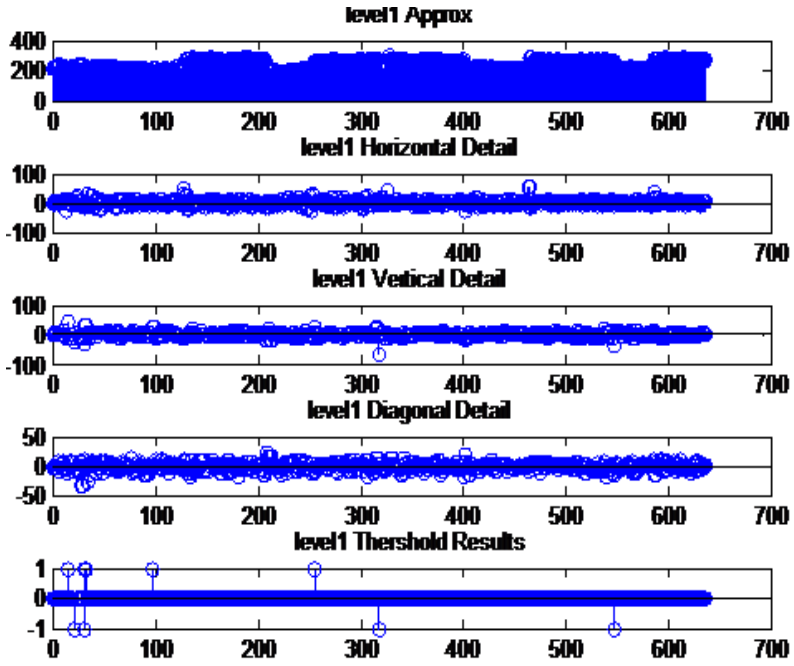

Fig.2.12 Plot of the line intensity approximation and detail coefficients after the Level 1 of SWT-based thresholding

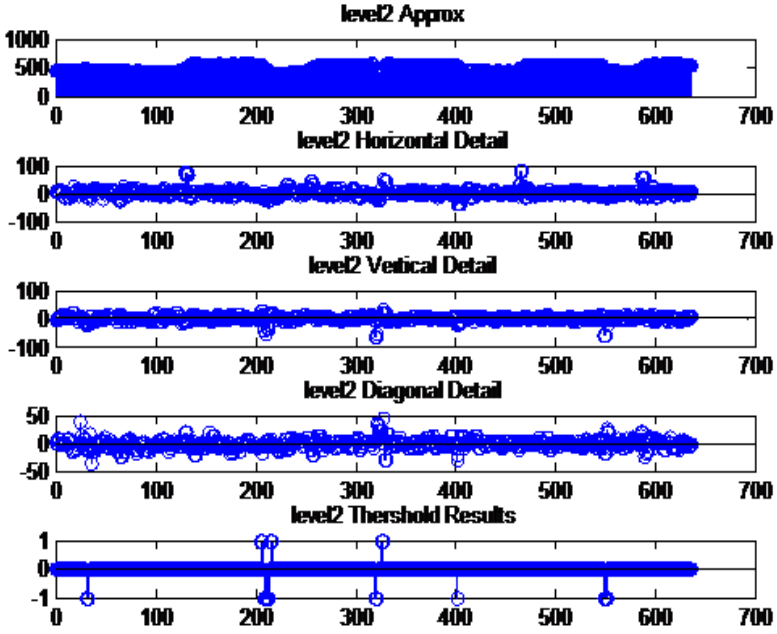

Fig.2.13 Plot of the line intensity approximation and detail coefficients after the Level 2 of SWT-based thresholding

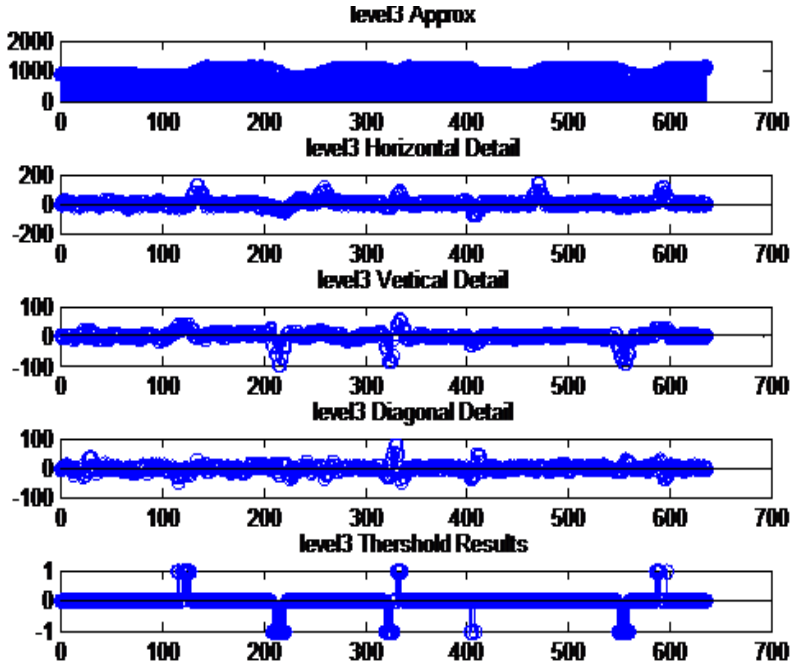

Fig.2.14 Plot of the line intensity approximation and detail coefficients after the Level 3 of SWT-based thresholding

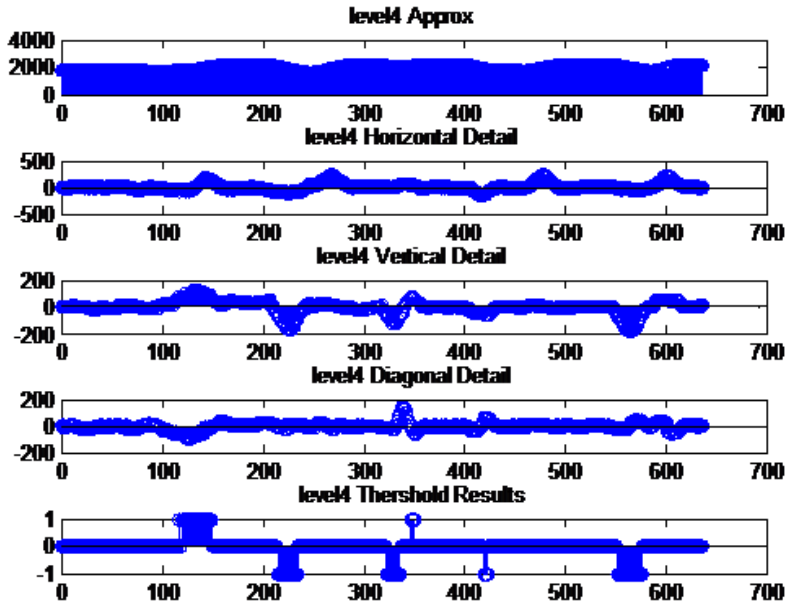

Fig.2.15 Plot of the line intensity approximation and detail coefficients after the Level 4 of SWT-based thresholding

We can observe that the 2D SWT-based de-noising and visualization offers more accurate representation than the thresholding based on 1D DWT. Additionally due to upsampling effect, which maintain the transform's time-shift invariance, the width of the resultant edge indicates the extent of the object boundary and thus can be used as an additional clue for further analyses.

One simple application of the measurable quantity can be the total number of retained coefficients. Divided by 2 and rounded this number represents a count of aggregates which the line is crossing. The spatial distances between retained coefficients of opposite signs represent lengths of cross sections of aggregates or pores, respectively. A more accurate way of quantifying these data is presented in Chapter 4.

CHAPTER 3

IMAGE SEGMENTATION

Component distribution around the root area and their geometry are important for quantification of the soil properties. Thus, segmentation is the next step in the processing data and preparing them for the analysis. In this Chapter we study the task of segmenting images for obtaining image components. The major components for the macro-scale analysis are soil pores, aggregates and the root. Additionally we have to subtract the container wall and the background. We implement various thresholding techniques and study their performance. Additionally we look for automated procedures for classification of the thresholding results and then conclude on the automated approach to move to an interactive method.

3.1 Image segmentation by means of thresholding

One of the conventional approaches for the task is to threshold images assuming that high grey-level represent, greater absorption incurred by the hard components, i.e., aggregates. Below we present the results from the major techniques that show thresholding of images. The originals are presented in Fig. 3.1 and the segmentation results are presented in Figures 3.2 and 3.3, respectively. In both Figure 3.2 and 3.3 the foreground is colored white and the background is presented by black pixels.

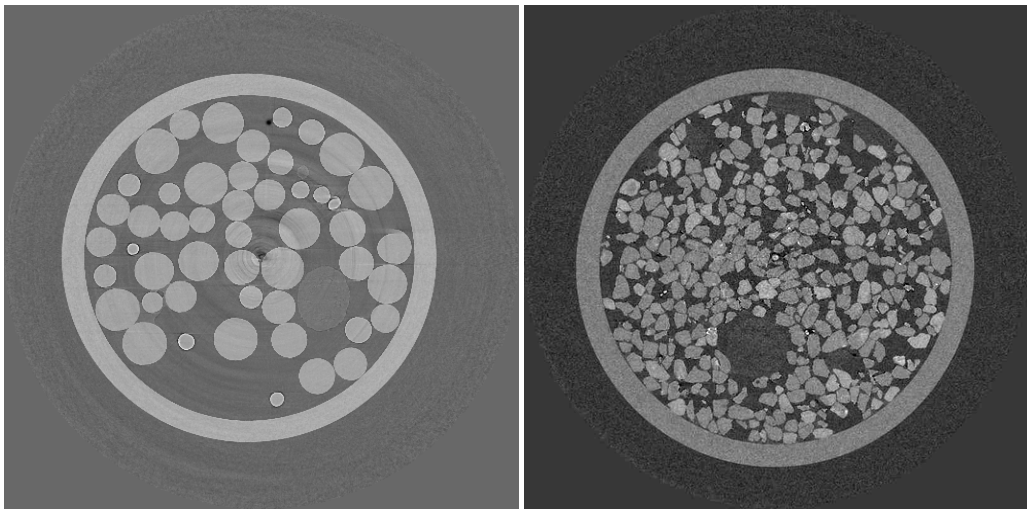

Fig.3.1 Original images

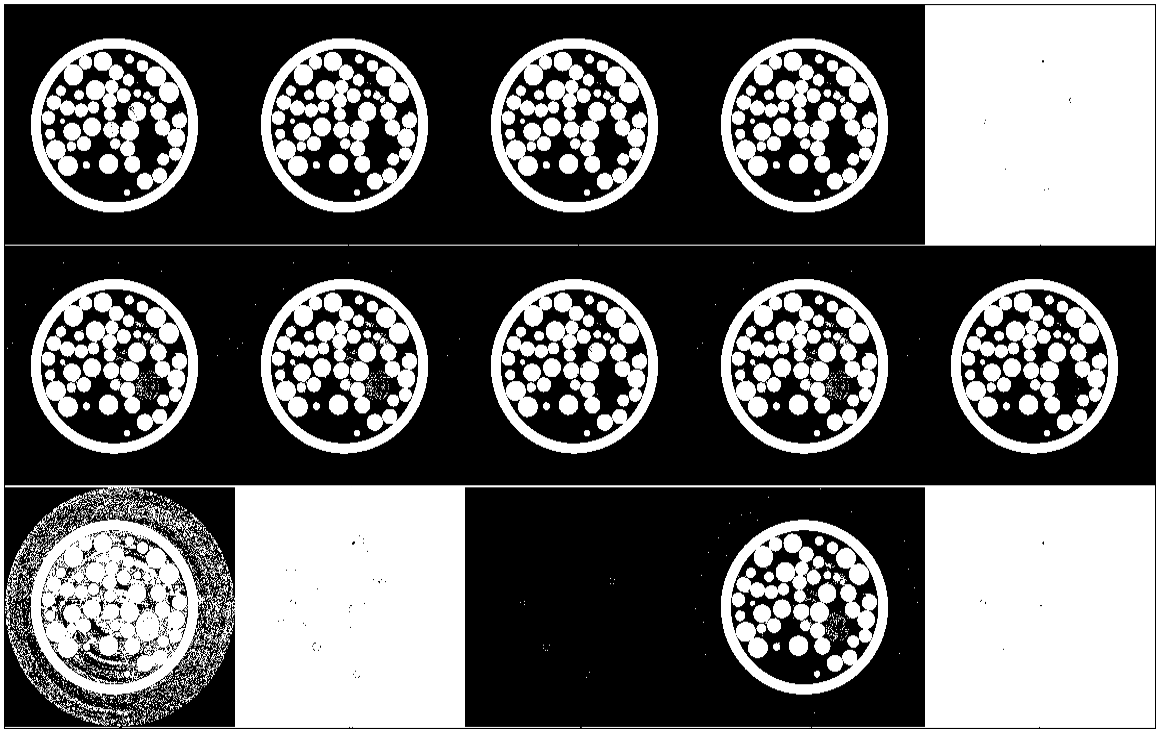

Fig. 3.2 Thresholding of Fig.3.1 (left): from left to right and top bottom sequence are Huang [27], Intermodes [28], IsoData [29], Li[30], MaxEntropy [31], Mean, MinError(I)

[32], Minimum [28], Moments [33], Otsu [34], Iterative thresholding[35], RenyiEntropy [31], Shanbhag [36], Triangle [37], Yen [38]

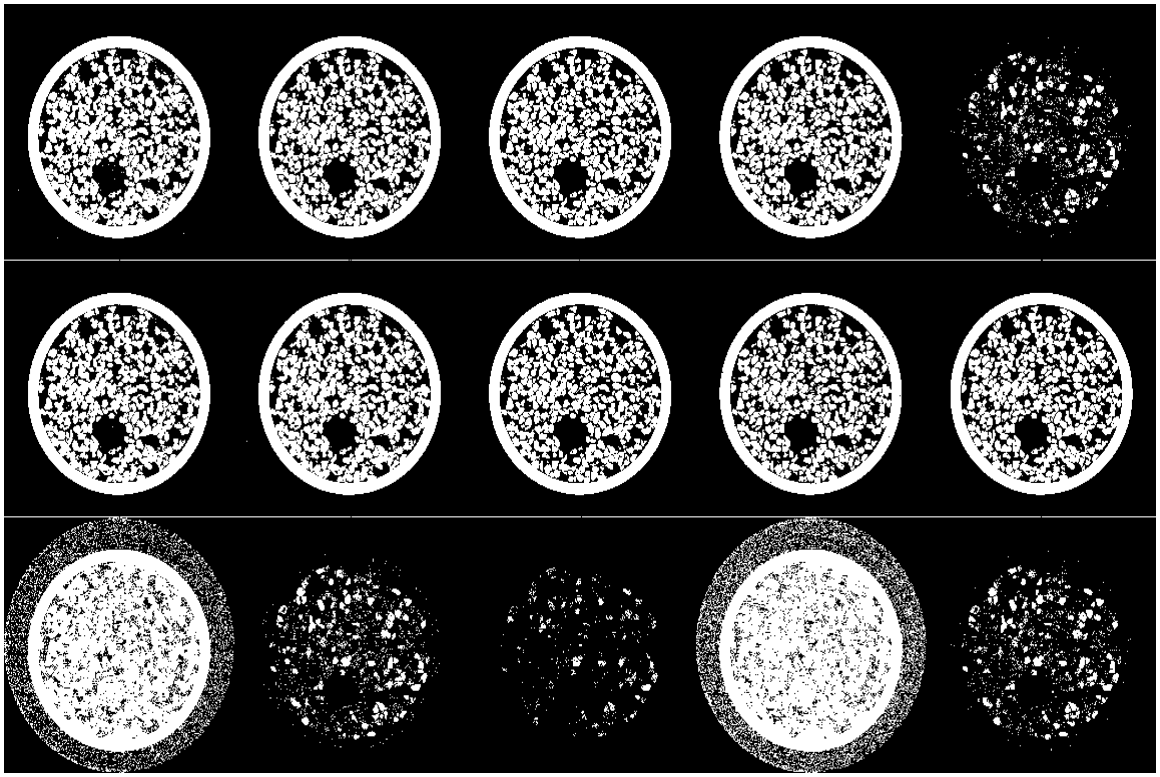

Fig. 3.3. Thresholding techniques applied to Fig.3.1(right): from left to right and top bottom sequence are form Huang, Intermodes, IsoData, Li, MaxEntropy, Mean, MinError(I), Minimum, Moments, Otsu, Iterative thresholding, RenyiEntropy, Shanbhag, Triangle, Yen

From the analysis it follows that techniques such as Huang, Intermodes, IsoData, Li Mean, MinError(I), Minimum, Moments, Otsu perform fairly well; however the root is not or barely distinguished from the rest of the pore area. Therefore in an attempt to

segment the root, one of the approaches here is to train a classifier such as a Neural Network based on the textures features as the image components(and the root in particular exhibits a certain and a distinguished texture type). For only root delineation, every pixel is to be classified as being a root or not a root pixel based on the features derived from a neighborhood. These can be a standard histogram features, i.e., mean, standard deviation, second and third moments. Although this approach allows for outlying the root area as it can be seen in Fig.3.4, but it takes a prohibitively long time on the images of the given resolution.

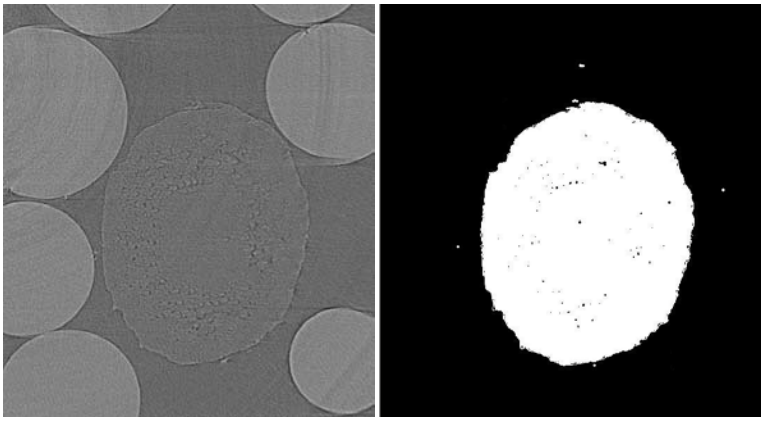

Fig.3.4. Left: Original around the root area Right: NN based root segmentation

To speed up the analysis we propose a simplistic approach which involves human interaction, but it is more accurate for fulfilling the goal.

3.2. Interactive procedures for obtaining image components

Taking into account the complexity of the automated procedures, we next consider a more feasible approach based on the human-machine interaction.

First, we perform k-means as it has shown the best performance among the thresholding techniques studied in this work. Next, we subtract the container wall. For that, a few points are selected on the inner part of that and line fitting is performed using cubic spline function. The outer part of the image is zeroed. Then, the same procedure is applied to the root surface and a mask of the root area is obtained. By logical OR operation the residual of the previous and the last steps are fused to produce a segmented image suitable for further analysis as shown in Figures.3.5 and 3.6

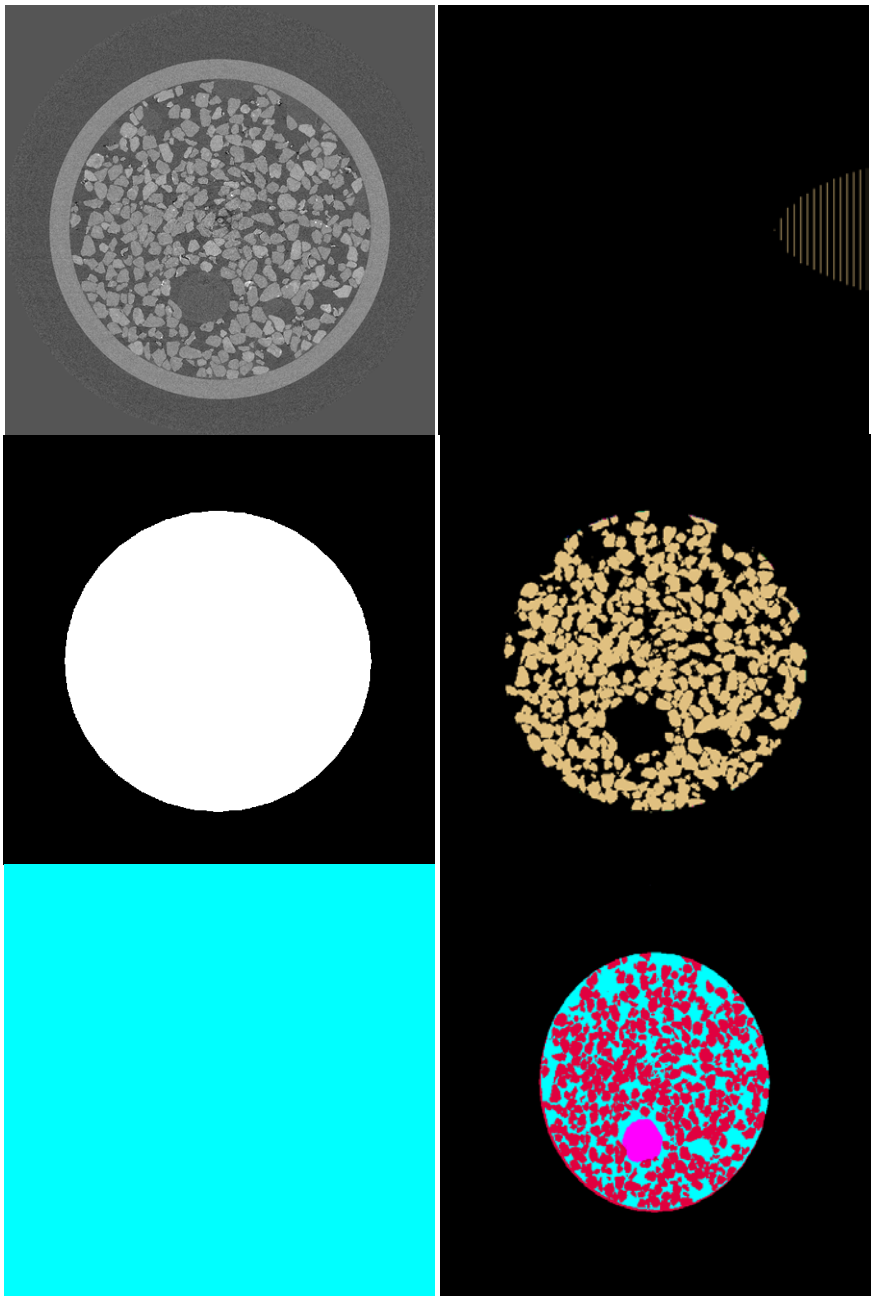

Fig.3.5.top-down, left-right: Original, Thresholded image, Container, Substracted image; Root mask; Final segmentation result

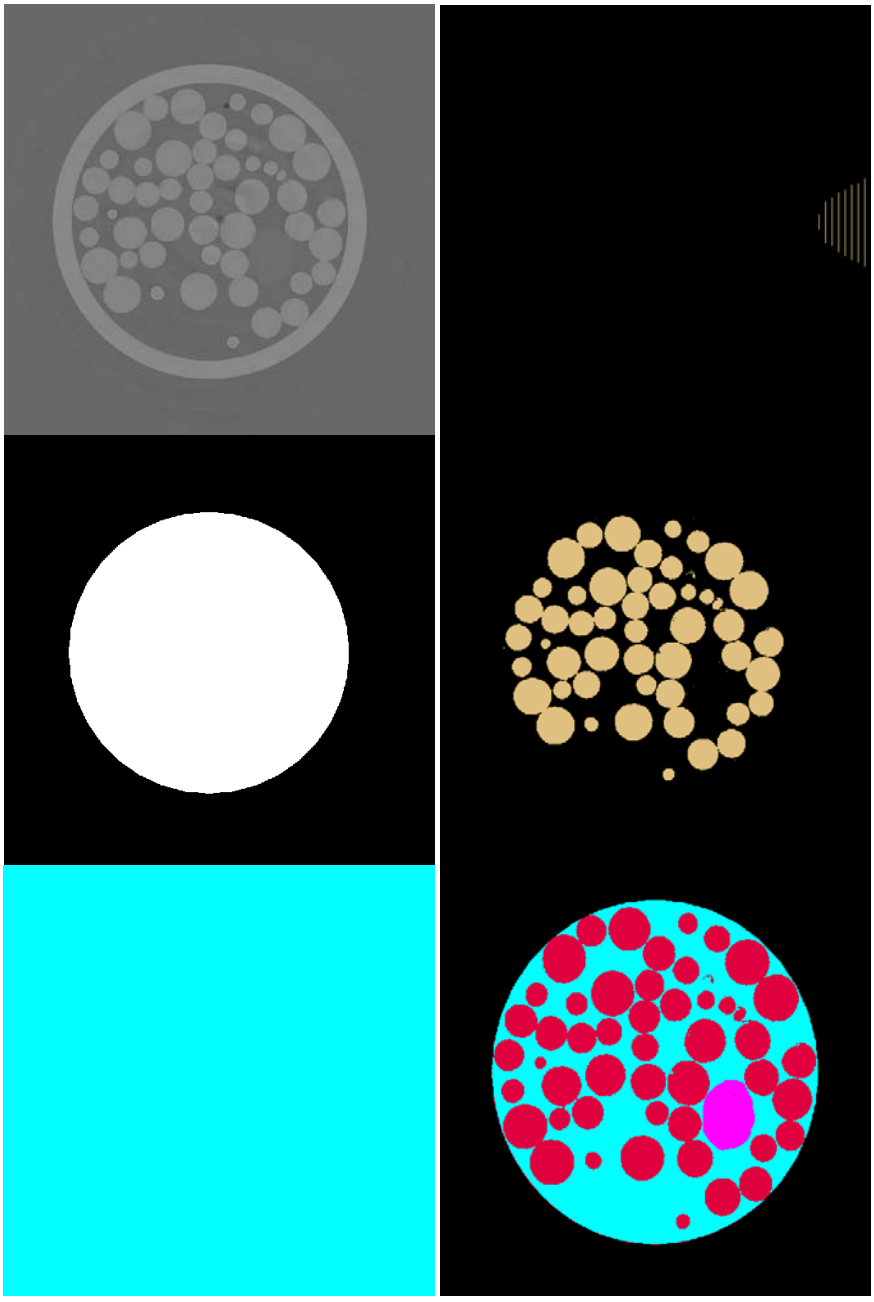

Fig.3.6 Top-down, left-right: Original, Thresholded image, Container, Subtracted image; Root mask; Final segmentation result

The segmented image is now suitable for macro-scale analysis, as it will be shown in the next Chapter.

CHAPTER 4

QUANTIFICATION OF MICROCT IMAGES

In this chapter, we introduce metrics of aggregation and measures which are found to be useful for characterizing the potential of the soil to transport the water to the root surface. We extend the analysis to 2D and also conclude on possible extension to 3D analyses.

4.1 Pore-Aggregate Area Distribution

We would like to obtain first the total aggregate/pore area at specified distances from the root. In order to quantify these measures interactively or automatically, we identify circular regions around the mass center of the root as shown in Figure 4.1, and then calculate aggregate and pore total area in a specified circle (see results in Table 4.1).

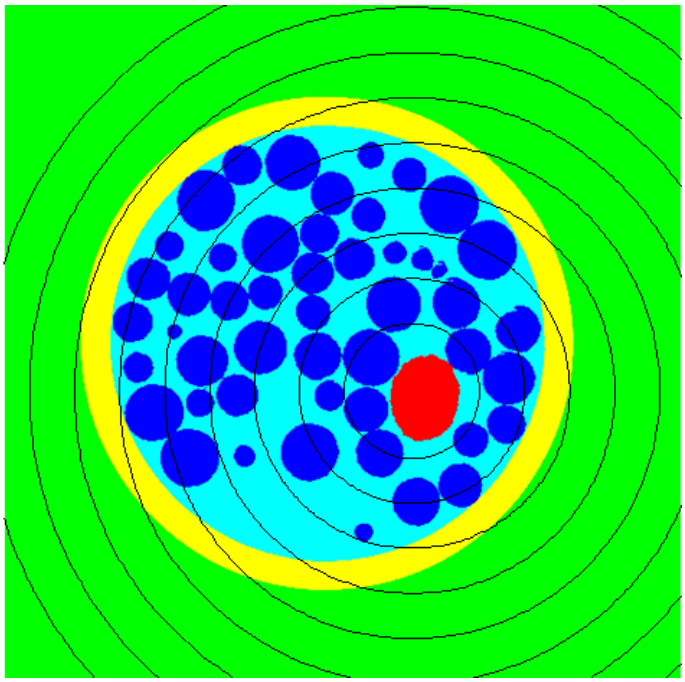

Fig.4.1. Concentric circles around the root center.

		gate
300	72740	86412
500	238328	343190
700	542327	533437
900	794355	745332
1100	1014828	950844
1300	1156539	1135418
1500	1199671	1165103
1700	1199672	1165103
1900	1199672	1165103

Table 4.1: Pore and Aggregate area distribution

For comparison, we obtain values normalized by the area of the circle as shown in Fig.4.2

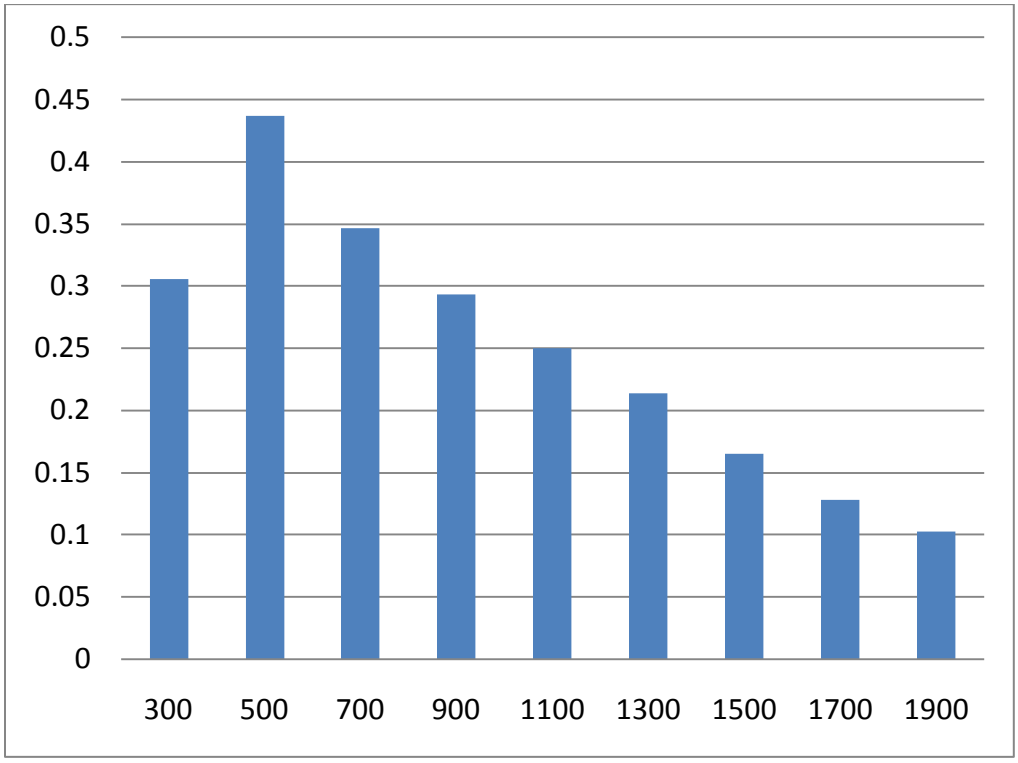

Fig.4.2 Normalized aggregate area (NAA)

A measure of inter-aggregate distances along the circumference line can be obtained and visualized as shown in Figures 4.3 and 4.4.

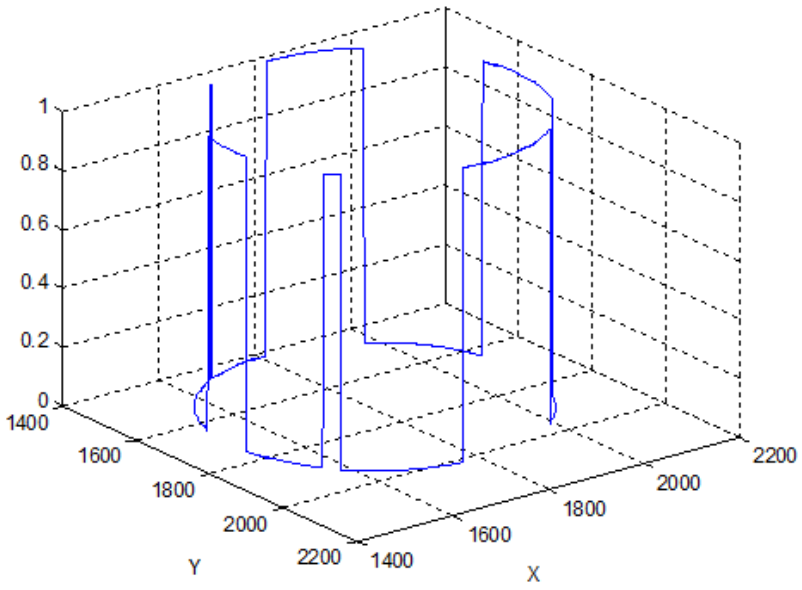

Fig.4.3 Aggregate/pore cross section (radius 300 pixels)

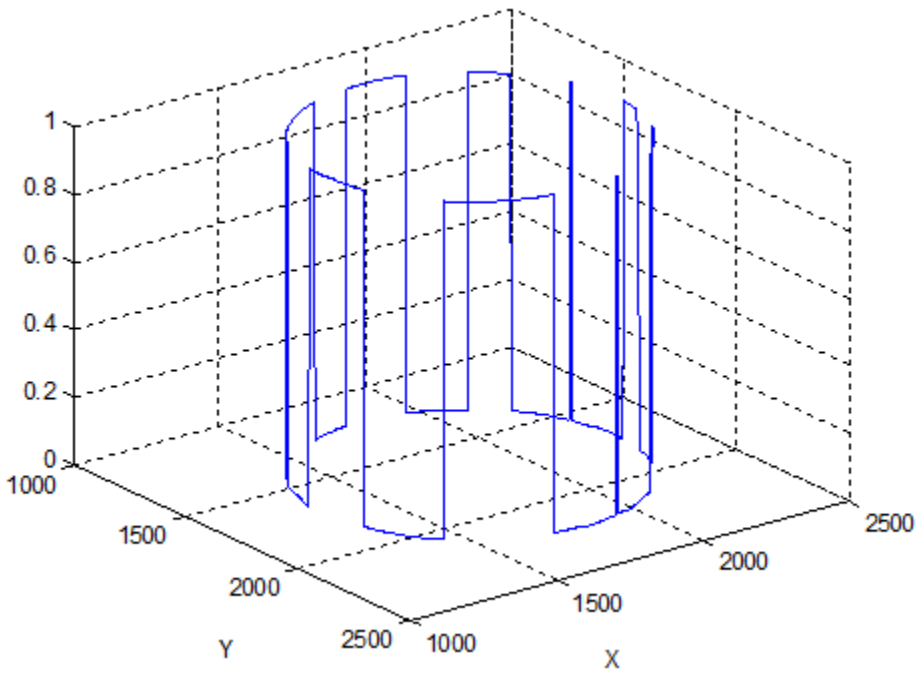

Fig.4.4 Aggregate/pore cross section (radius 500 pixels)

We propose another important characteristic which is the distance-to-aggregate radial (DAR) profile. It is calculated in the radial direction, as we believe that properties of soil compaction in a cylindrical container are likely isotropic with respect to the root vertical axis. From the mass center of the root, we draw 360 lines (one degree increments) and calculate distances from the root surface to the first aggregate along the lines. The plot in Fig. 4.5 is bounded by the maximum distance from the root surface to the container wall.

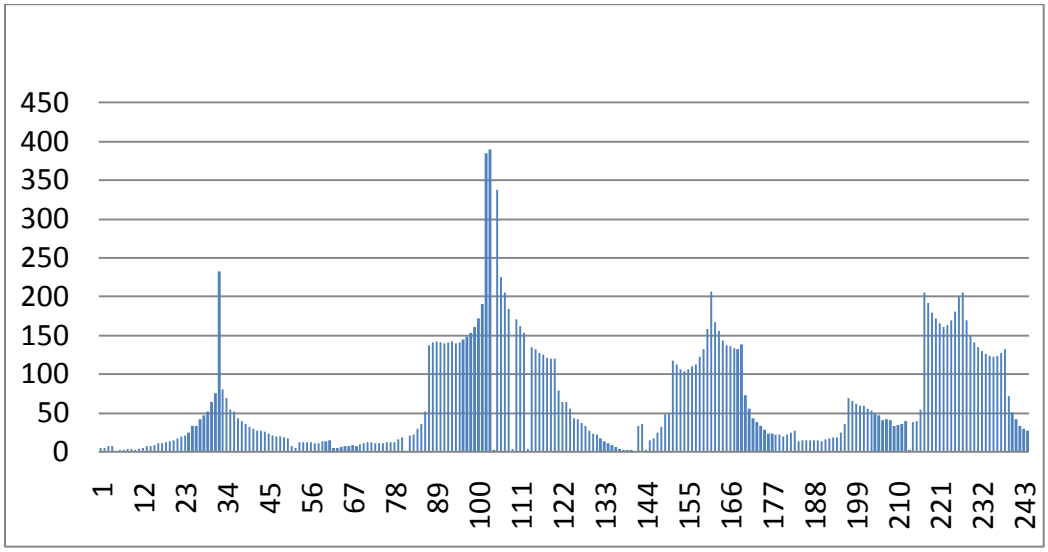

Fig.4.5 DAR profile

4.1.1 Normalized Radial Aggregation

Next we introduce Normalized Radial Aggregation (NRA) which we define as below:

$$NRA = \frac{\sum_{(i)} L_{CS_i}}{L}$$

The numerator in the above expression is the sum of cross sections along the radial lines as in the DAR metric; the denominator has a normalization factor L which is a length of the line from the root surface to the container wall as explained in Figure 4.6.

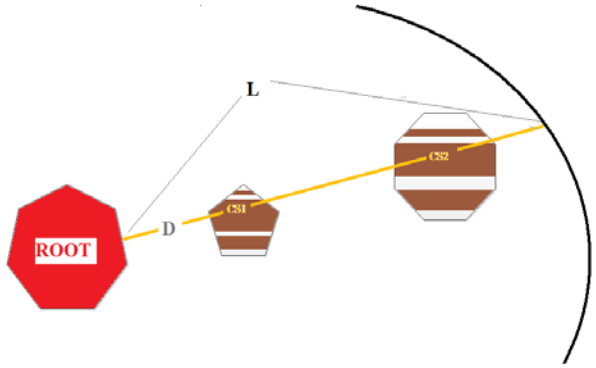

Figure 4.6

The NRA profile is presented in Fig.4.7.

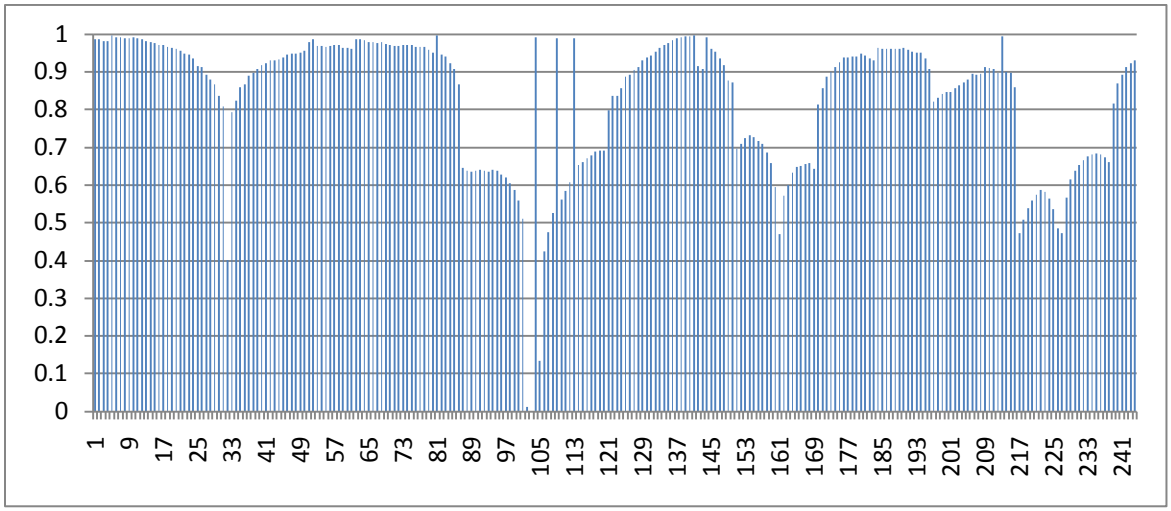

Fig.4.7 NRA profile

4.1.2 Normalized Water Transportability

To characterize the hydrological conductivity, we next introduce the following quantity that we name as normalized radial water transportability (NRWT):

$$NRWT = \frac{\sum_{(i)} L_{CS_i}}{L \cdot D}$$

where D is the distance to the first aggregate in a radial line act as a scaling factor. For the immediate contact case, it is assumed to be 1. Examples of this measure for the lines in two sectors depicted in Figure 4.8 are shown in Figures 4.9 and 4.10 respectively.

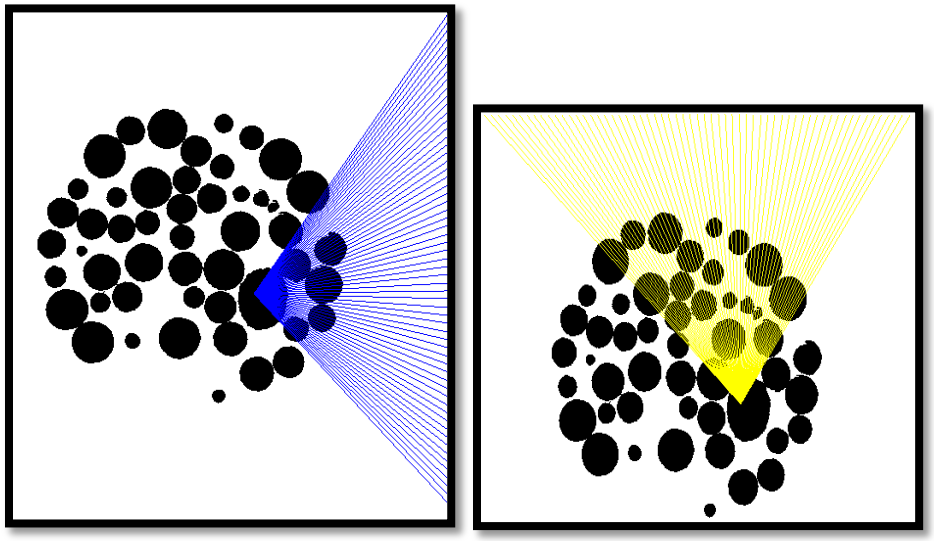

Fig 4.8 Two sectors of interest.

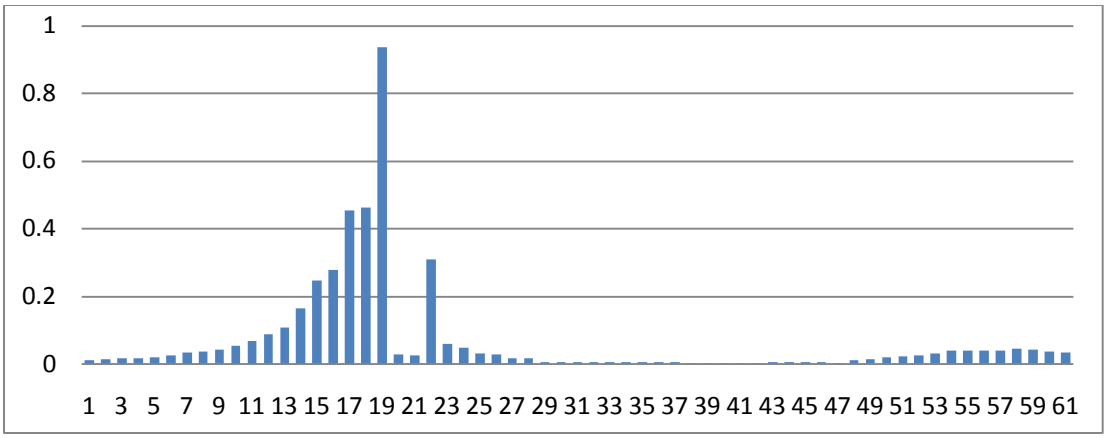

Fig.4.9. NRWT for lines depicted in Fig.4.8 (left)

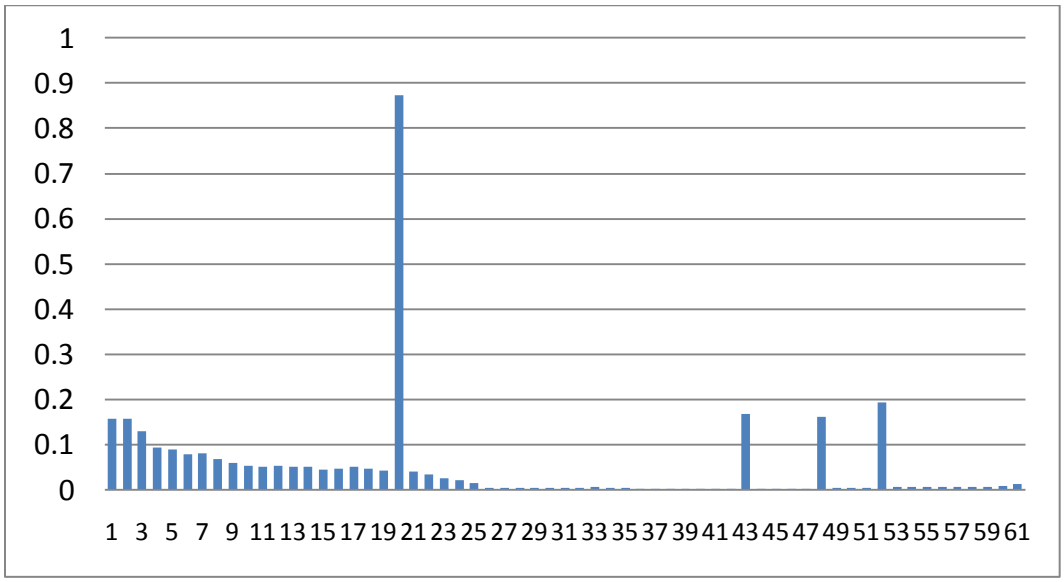

Fig.4.9. NRWT for lines depicted in Fig.4.8 (right)

This measure is further modified to use area as a property to represent water conductivity given by a formula below, where the areas of aggregates in the respective sectors are summed, scaled by a minimum distance to the aggregate in the sector and normalized by the sector area.

$$NSWT = \frac{\sum_{(i)} A_{CS_i}}{D_{\min}} \cdot \frac{1}{A_{sector}}$$

One can also derive the total contact area of soil-root and aggregate-root interface, and also observe the dynamics of aggregate compaction through analysis and quantification of time series. It can also be shown that metrics derived for 2D can be extended to a stack of slices and quantified in a same manner to obtain 2.5D measures.

CHAPTER 5

CONCLUSIONS AND THE FUTURE WORK

In this work we have presented image processing techniques that visualize and analyze microCT images for soil-root interaction studies. Intensity profile enhancement for visual and quantitative analysis of soil properties and hydrological conductivity are proposed and demonstrated. Then we have studied data pre-processing for image quantification. Specifically an efficient interactive procedure is developed for segmenting images into components necessary for image quantification. Lastly, various useful metrics of aggregation and those characterizing the water transport potential of the soil. The normalized measures can be used for comparison. Also, obtained for a 2D slice, these measures can be similarly extended to a stack of images yielding 2.5D measures.

The outcome of this study provides a first step towards transformative insights into the role of rhizosphere physical properties for water and nutrient uptake by living plants. It serves as a stepping stone for better understanding the role of plants in the critical zone at the soil-atmosphere interface. The value of this work is also in the development of semi-automated procedures which assist experts in image analysis and quantification. The results of this work represent a first phase effort towards the development of a tailored software tool which will combine preprocessing, processing and analysis steps and will include a set of various procedures which can be applied in combinations to attain better results at expert's opinion. For example other shrinkage functions for wavelet-based de-noising can be included, elimination of hard components seen as very bright spots can be implemented based on histogram-based thresholding or morphological filtering. Segmentation algorithms based on clustering of texture features

(feature vectors in fact) can be incorporated. We also envision inclusion of 3D visualization and 3D segmentation, and that will demand on 3D metrics of soil properties and hydrological conductivity. A graph-theoretical approach to study water flow on a graph model of the soil is another interesting area of the research which can be pursued.

The problems solved in this work cut across disciplinary boundaries of biology, soil physics, and soil mechanics to offer new insights on surface runoff, soil compaction and erosion, losses to agricultural productivity, land reclamation, and first-principles of soil-plant interactions. The task of this work is to apply engineering methods specifically image processing and analysis techniques to perform studies on the physical properties of soil for understanding soil-root interfacing mechanism from imagery.

REFERENCES

[1] L. Hiltner, "Über neuere Erfahrungen und Probleme auf dem Gebiete der Bodenbakteriologie unter besonderer Berücksichtigung der Gründüngung und Brache," *Arbeiten der Deutschen Landwirtschaftlichen Gesellschaft,* vol. 98, pp. 59–78, 1904.

[2] I. M. Young, "Biophysical interactions at the root-soil interface: a review," *Journal of Agricultural Science,* vol. 130, pp. 1-7, 1998.

[3] Y. Dessaux, P. Hinsinger, and P. Lemanceau, "Rhizosphere: Achievements and Challenges " in *Developments in Plant and Soil Sciences*: Springer, 2009, p. 538.

[4] P. J. Gregory, "Roots, rhizosphere and soil: the route to a better understanding of soil science?," *European Journal of Soil Science,* vol. 57, pp. 2-12, Feb 2006.

[5] P. Hinsinger, A. G. Bengough, D. Vetterlein, and I. A. Young, "Rhizosphere: biophysics, biogeochemistry and ecological relevance," *Plant and Soil,* vol. 321, pp. 117–152, 2009.

[6] P. Hinsinger, C. Plassard, and B. Jaillard, "Rhizosphere: A new frontier for soil biogeochemistry," *Journal of Geochemical Exploration* vol. 88, pp. 210-213, 2006.

[7] M. Berli, M. Menon, T. A. Ghezzehei, N. S. Pillai, E. E. Regentova, P. S. Nico, M. H. Young, and S. W. Tyler, "Quantifying Rhizosphere Soil Structure Alterations using X-Ray Micro-Tomography and Image Analysis," *Vadose Zone Hydrology,* p. submitted, 2010.

[8] R. A. Ketcham and W. D. Carlson, "Acquisition, optimization and interpretation of X-ray computed tomographic imagery: applications to the geosciences," *Computers & Geosciences,* vol. 27, pp. 381-400, 2001.

[9] A. Kaestner, E. Lehmann, and M. Stampanoni, "Imaging and image processing in porous media research," *Advances in Water Resources,* vol. 31, pp. 1174-1187, 2008.

[10] R. Hassanein, H. O. Meyer, A. Carminati, M. Estermann, E. Lehmann, and P. Vontobel, "Investigation of water imbibition in porous stone by thermal neutron radiography," *Journal of Physics D-Applied Physics,* vol. 39, pp. 4284-4291, Oct 2006.

[11] P. Iassonov, T. Gebrenegus, and M. Tuller, "Segmentation of X-ray computed tomography images of porous materials: A crucial step for characterization and quantitative analysis of pore structures," *Water Resour. Res.,* vol. 45, p. W09415, 2009.

[12] M. Porter and D. Wildenschild, "Image analysis algorithms for estimating porous media multiphase flow variables from computed microtomography data: a validation study," *Computational Geosciences,* vol. 14, pp. 15-30, 2010.

[13] D. Wildenschild, J. W. Hopmans, M. L. Rivers, and A. J. R. Kent, "Quantitative Analysis of Flow Processes in a Sand Using Synchrotron-Based X-ray Microtomography." vol. 4, 2005, pp. 112-126.

[14] P. Lehmann, P. Wyss, A. Flisch, E. Lehmann, P. Vontobel, M. Krafczyk, A. Kaestner, F. Beckmann, A. Gygi, and H. Fluhler, "Tomographical Imaging and Mathematical Description of Porous Media Used for the Prediction of Fluid Distribution." vol. 5, 2006, pp. 80-97.

[15] I. A. Taina, R. J. Heck, and T. R. Elliot, "Applications of X-ray computed tomography to soil science: A literature review," *Canadian Journal of Soil Science,* vol. 88, pp. 1-20, 2008.

[16] C. J. Moran, A. Pierret, and A. W. Stevenson, "X-ray absorption and phase contrast imaging to study the interplay between plant roots and soil structure," *Plant and Soil,* vol. 223, pp. 99-115, 2000.

[17] A. Pierret, M. Kirby, and C. Moran, "Simultaneous X-ray imaging of plant root growth and water uptake in thin-slab systems," *Plant and Soil,* vol. 255, pp. 361-373, Aug 2003.

[18] M. Menon, S. Hermle, M. S. Gunthardt-Goerg, and R. Schulin, "Effects of heavy metal soil pollution and acid rain on growth and water use efficiency of a young model forest ecosystem," *Plant and Soil,* vol. 297, pp. 171-183, Aug 2007.

[19] S. E. Oswald, M. Menon, A. Carminati, P. Vontobel, E. Lehmann, and R. Schulin, "Quantitative imaging of infiltration, root growth, and root water uptake via neutron radiography," *Vadose Zone Journal,* vol. 7, pp. 1035-1047, Aug 2008.

[20] A. Pohlmeier, A. Oros-Peusquens, M. Javaux, M. I. Menzel, J. Vanderborght, J. Kaffanke, S. Romanzetti, J. Lindenmair, H. Vereecken, and N. J. Shah, "Changes in soil water content resulting from Ricinus root uptake monitored by magnetic resonance Imaging," *Vadose Zone Journal,* vol. 7, pp. 1010-1017, 2008.

[21] P. J. Gregory, D. J. Hutchison, D. B. Read, P. M. Jenneson, W. B. Gilboy, and E. J. Morton, "Non-invasive imaging of roots with high resolution X-ray micro-tomography," *Plant and Soil*, vol. 255, pp. 351-359, Aug 2003.

[22] C. E. Hargreaves, P. J. Gregory, and A. G. Bengough, "Measuring root traits in barley (Hordeum vulgare ssp. vulgare and ssp. spontaneum) seedlings using gel chambers, soil sacs and X-ray microtomography," *Plant and Soil*, vol. 316, pp. 285–297, 2009.

[23] K. G. Schecke, R. Hamon, L. Jassogne, M. Rivers, and E. Lombi, "Synchrotron X-ray absorption-edge computed microtomography imaging of thallium compartmentalization in Iberis intermedia," *Plant and Soil*, vol. 290, pp. 51-60, 2006.

[24] A. J. Devaney, "A Fast Filtered Backpropagation Algorithm for Ultrasound Tomography," *Ultrasonics, Ferroelectrics and Frequency Control, IEEE Transactions on*, vol. 34, pp. 330-340, 1987.

[25] M. Sezgin and B. Sankur, "Survey over image thresholding techniques and quantitative performance evaluation," *Journal of Electronic Imaging*, vol. 13, pp. 146-168, 2004.

[26] A. L. C. H. Arne Jensen, Ripples in Mathematics : The Discrete Wavelet Transform: Springer, 2001.

[27] W. Qing, C. Zheru, and Z. Rongchun, "Image thresholding by maximizing the index of nonfuzziness of the 2-D grayscale histogram." vol. 85: Elsevier Science Inc., 2002, pp. 100-116.

[28] M. S. P. Judith and L. M. Mortimer, "THE ANALYSIS OF CELL IMAGES*." vol. 128, 1965, pp. 1035-1053.

[29] "Picture Thresholding Using an Iterative Selection Method," *Systems, Man and Cybernetics, IEEE Transactions on*, vol. 8, pp. 630-632, 1978.

[30] C. H. Li and C. K. Lee, "Minimum cross entropy thresholding," *Pattern Recognition*, vol. 26, pp. 617-625, 1993.

[31] J. N. Kapur, P. K. Sahoo, and A. K. C. Wong, "A new method for gray-level picture thresholding using the entropy of the histogram," *Computer Vision, Graphics, and Image Processing*, vol. 29, pp. 273-285, 1985.

[32] J. Kittler and J. Illingworth, "Minimum error thresholding." vol. 19: Elsevier Science Inc., 1986, pp. 41-47.

[33] T. Wen-Hsiang, "Moment-preserving thresholding: a new approach," in *Document image analysis*: IEEE Computer Society Press, 1995, pp. 44-60.

[34] N. Otsu, "A threshold selection method from gray-level histograms," *IEEE Transactions on Systems, Man and Cybernetics*, vol. 9, pp. 62-66, 1979.

[35] P. Arnulfo, rez, and C. G. Rafael, "An iterative thresholding algorithm for image segmentation." vol. 9: IEEE Computer Society, 1987, pp. 742-751.

[36] G. S. Abhijit, "Utilization of information measure as a means of image thresholding." vol. 56: Academic Press, Inc., 1994, pp. 414-419.

[37] G. W. Zack, W. E. Rogers, and S. A. Latt, "Automatic measurement of sister chromatid exchange frequency." vol. 25, 1977, pp. 741-753.

[38] Y. Jui-Cheng, C. Fu-Juay, and C. Shyang, "A new criterion for automatic multilevel thresholding," *Image Processing, IEEE Transactions on*, vol. 4, pp. 370-378, 1995.

VITA

Graduate College
University of Nevada, Las Vegas

Natarajan Sivathanu Pillai

Degree:

Bachelor of Engineering, Electronics and Communication Engineering, 2006, Anna University, India

Publications:

Pillai N.S, D.Sheela, and S. Ananthi, 2008. Hardware Optimization for Image Compression with JPEG2000 Core Coding System. Journal of Instrument Society of India, Vol. 38(2): 145-155.

Thesis Title:

Automated Proceedures for Quantification of Rhizosphere Physical Properties in Micro CT images.

Thesis Examination Committee:

Committee Chair, Dr. Emma E. Regentova, Ph.D.
Committee Member, Dr.Peter Allen Stubberud, Ph.D.
Committee Member, Dr. Henry Selvaraj, Ph.D.
Committee Member, Dr.Markus Berli Ph.D.
Graduate College Representative, Dr. Ajoy Kumar Datta, Ph.D.